Supplementary Methods

Design and fabrication of the microfluidic perfusion device. The microfluidic device for superfusing RBCs consisted of two input lines, each branching into a system of eight capillary channels laid on a plane of two circles. The channels delivered solution to a central circular observation chamber (2.4 mm diameter and 0.2 mm height) with an open bottom, onto which a coverslip is attached for allowing cells to settle. The internal three-step bifurcation tree divides the flow of solution equally by a factor of eight. This ensured that the delivery to the observational chamber was rotationally symmetrical. Such an arrangement of channels ensured uniform delivery of solution to cells, irrespective of their position in the central inspection zone. The number of feeding channels was constrained by the dimensions of the inspection zone and channel width. Considering these constraints, 8 channels emerging per line was an optimal design: fewer lines could make solution exchange less uniform and more lines could make the circuit unnecessarily complicated to manufacture and more prone to bubble formation. The bifurcation trees were designed for each line independently and were arranged on separate layers of the microfluidic device. Access was via vertical stainless-steel tubes. Solution exits from the chamber through a vertical vent at the centre of the observation chamber. The microfluidic device was fabricated by engraving channels and structures in transparent, polycarbonate plates (Makrolon® GP, Bayer, Germany) using a CNC milling machine (MFG4025P, Ergwind, Gdansk, Poland) and a 2-flute fishtail milling bit with a diameter of 385 µm (FR208, InGraph, Goleniow, Poland). Channels were cleaned with a high-pressure water washer (Karcher, K7 Premium, Winnenden, Germany) to remove turnings and loosely bound bulk material formed during the milling process. Further, the milled chips were washed with 1% water solution of Alconox detergent (Alconox Inc., White Plains, NY, USA), isopropanol, deionized water and finally dried with compressed air. Polycarbonate plates were then bonded to form a monolith device with a network of closed channels using a hot press (AW03, Argenta, Poznan, Poland) at a temperature of 135 °C and with 0.1 bar/cm2 pressure. The chip was kept in the press at this high temperature for 10 min and then allowed to cool down remaining under pressure. To prevent the formation of air bubbles, polycarbonate channels were hydrophilized (1).

Delivery of solutions to the microfluidic chamber. Superfusates were delivered by gravity from bottles positioned ~35 cm above the apparatus and fed through 1 mm-internal diameter versilic silicone tubing (Saint-Gobain, Paris, France) to the inputs of the chamber. The hypoxic line was encapsulated in a gas permeable tube of a larger diameter through which N_2 gas

was flushed to prevent oxygen ingress from the atmosphere. The design of the microfluidic chamber is compatible with fast solution flows (2.25 ml/min per line) and exchanges. To alternate rapidly between solutions, the flow in each of the two lines was controlled by an electromagnetic valve (V165, equipped with Z070D coils, Sirai, Italy). The valve controlling the hypoxic line was enclosed in a casing flushed with N_2 gas which then fed into the solution reservoir and the rest of the tubing. Valves were operated by Raspberry Pi Pico (Rasberry Pi Foundation, Cambridge, Great Britain) using H-bridge motor driver (A4990 Dual Motor Driver Carrier, Pololu, USA). The control was exercised via the USB connection and custom-built software that allows applying a user-defined sequence of flow switching protocols.

Single-cell oxygen saturation imaging. This fluorescence-based assay measures the time constant and relative degree of O_2-unloading evoked by a period of anoxia. Blood was first diluted 1000-fold in Hepes-buffered Tyrode, containing (in mM): 130 NaCl, 4.5 KCl, 1 $CaCl_2$, 1 $MgCl_2$, 5 glucose, 20 Hepes, pH adjusted to 7.4 (at room temperature) with 4M NaOH. All salts were obtained from Sigma-Aldrich (Dorset, UK). Diluted red cells were loaded with a mixture of CellTracker Deep Red (final concentration 4 μM) and Calcein (final concentration 16 μM) permeant dyes in 4 mM stock (ThermoFisher Scientific, Massachusetts, USA) in dimethyl sulfoxide (DMSO). Red cells were incubated in the dark for 10 min for dye loading prior to being pelleted and resuspended in fresh Hepes-buffered Tyrode. Stained red cells were plated onto poly-L-lysine (Sigma-Aldrich, Dorset, UK) pre-treated borosilicate coverslips attached to the base of the microfluidic chamber. Cells were superfused with alternating streams of anoxic and normoxic Hepes-buffered Tyrode solutions at 23°C. Anoxic solution was achieved by supplementing Hepes-buffered Tyrode with 2 mM sodium dithionite and continuous bubbling with N_2. Excitation was delivered at 640 and 488 nm and the fluorescence signal was split by a dichroic mirror to image red and green channels simultaneously with a W-view Gemini (Hamamatsu, Welwyn Garden City, UK). Images were acquired using a Hamamatsu ORCA-Flash4.0 camera (Hamamatsu, Welwyn Garden City, UK). Integration time for green fluorescence was 200 ms, and adjusted between 20 and 50 ms for red fluorescence, such that the ratio was close to one. For each field of view, three anoxic intervention were performed (technical repeat) and up to five fields of view were imaged per loading. For each condition, at least two loadings were performed. Images were analyzed offline using a custom-made macro that identified red cells by particle analyses, and ratioed the signals after background subtraction. The time courses were fitted with a mono-exponential curves that defined the time constant and degree of change.

Metabolomics. Metabolomics analyses were performed as described previously (2-4). 50 µl frozen RBC aliquots were extracted in 450µl of methanol:acetonitrile:water (5:3:2, v/v/v).

After vortexing at 4°C for 30 min, extracts were separated from the protein pellet by centrifugation for 10 min at 10,000g at 4°C and stored at −80°C until analysis. Ultra-high pressure liquid chromatography-mass spectrometry analyses were performed using a Vanquish UHPLC coupled online to a Q Exactive mass spectrometer (ThermoFisher, Bremen, Germany). Samples were analyzed using a 5-minute gradient (5). Solvents were supplemented with 0.1% formic acid for positive mode runs and 1 mM ammonium acetate for negative mode runs. Statistical analyses were performed with MetaboAnalyst 5.0 (6).

Lipidomics Lipidomics analyses were performed via UHPLC-MS/MS, as previously described in technical notes (7) and RBC storage studies (2).

Proteomics and post-translational modifications Proteomics analyses were performed via FASP digestion and nanoUHPLC-MS/MS identification (TIMS TOF Pro 2 Single Cell Proteomics, Bruker Daltonics, Bremen, Germany), as previously described (8).

Additional references

1. Jankowski P, Ogonczyk D, Kosinski A, Lisowski W, Garstecki P. Hydrophobic modification of polycarbonate for reproducible and stable formation of biocompatible microparticles. Lab Chip. 2011 Feb 21;11(4):748-52. Epub 20101206. doi:10.1039/c0lc00360c. Cited in: Pubmed; PMID 21132214.

2. Stefanoni D, Shin HKH, Baek JH, Champagne DP, Nemkov T, Thomas T, Francis RO, Zimring JC, Yoshida T, Reisz JA, Spitalnik SL, Buehler PW, D'Alessandro A. Red blood cell metabolism in Rhesus macaques and humans: comparative biology of blood storage. Haematologica. 2020 Aug;105(8):2174-2186. Epub 2019/11/09. doi:10.3324/haematol.2019.229930. Cited in: Pubmed; PMID 31699790.

3. Nemkov T, Stefanoni D, Bordbar A, Issaian A, Palsson BO, Dumont LJ, Hay AM, Song A, Xia Y, Redzic JS, Eisenmesser EZ, Zimring JC, Kleinman S, Hansen KC, Busch M, D'Alessandro A. Blood donor exposome and impact of common drugs on red blood cell metabolism. JCI Insight. 2020 Dec 22. Epub 2020/12/23. doi:10.1172/jci.insight.146175. Cited in: Pubmed; PMID 33351786.

4. D'Alessandro A, Fu X, Kanias T, Reisz JA, Culp-Hill R, Guo Y, Gladwin MT, Page G, Kleinman S, Lanteri M, Stone M, Busch MP, Zimring JC, Recipient E, Donor Evaluation S, III. Donor sex, age and ethnicity impact stored red blood cell antioxidant metabolism through mechanisms in part explained by glucose 6-phosphate dehydrogenase levels and activity. Haematologica. 2020 Apr 2. Epub 2020/04/04. doi:10.3324/haematol.2020.246603. Cited in: Pubmed; PMID 32241843.

5. Nemkov T, Reisz JA, Gehrke S, Hansen KC, D'Alessandro A. High-Throughput Metabolomics: Isocratic and Gradient Mass Spectrometry-Based Methods. Methods Mol

Biol. 2019;1978:13-26. Epub 2019/05/24. doi:10.1007/978-1-4939-9236-2_2. Cited in: Pubmed; PMID 31119654.

6. Pang Z, Chong J, Zhou G, de Lima Morais DA, Chang L, Barrette M, Gauthier C, Jacques P, Li S, Xia J. MetaboAnalyst 5.0: narrowing the gap between raw spectra and functional insights. Nucleic Acids Res. 2021 Jul 2;49(W1):W388-w396. eng. Epub 2021/05/22. doi:10.1093/nar/gkab382. Cited in: Pubmed; PMID 34019663.

7. Reisz JA, Zheng C, D'Alessandro A, Nemkov T. Untargeted and Semi-targeted Lipid Analysis of Biological Samples Using Mass Spectrometry-Based Metabolomics. Methods Mol Biol. 2019;1978:121-135. Epub 2019/05/24. doi:10.1007/978-1-4939-9236-2_8. Cited in: Pubmed; PMID 31119660.

8. Thomas T, Stefanoni D, Dzieciatkowska M, Issaian A, Nemkov T, Hill RC, Francis RO, Hudson KE, Buehler PW, Zimring JC, Hod EA, Hansen KC, Spitalnik SL, D'Alessandro A. Evidence for structural protein damage and membrane lipid remodeling in red blood cells from COVID-19 patients. medRxiv. 2020 Jun 30. Epub 2020/07/09. doi:10.1101/2020.06.29.20142703. Cited in: Pubmed; PMID 32637980.

Supplementary Video 1: Video showing exchange of clear and dye-stained (blue) solution in the microfluidic chamber.

Supplementary Table S1: Demographic and haemoglobin levels in venous blood (HemaCue) in six donors giving venous blood for reference values.

Supplementary Table S2: List of differentially abundant metabolites that are affected by hypoxic storage and/or biochemical rejuvenation and are plotted in Figure 5B.

Supplementary Table S3: List of differentially abundant metabolites that are affected by hypoxic storage and/or biochemical rejuvenation and are plotted in Figure 5H.

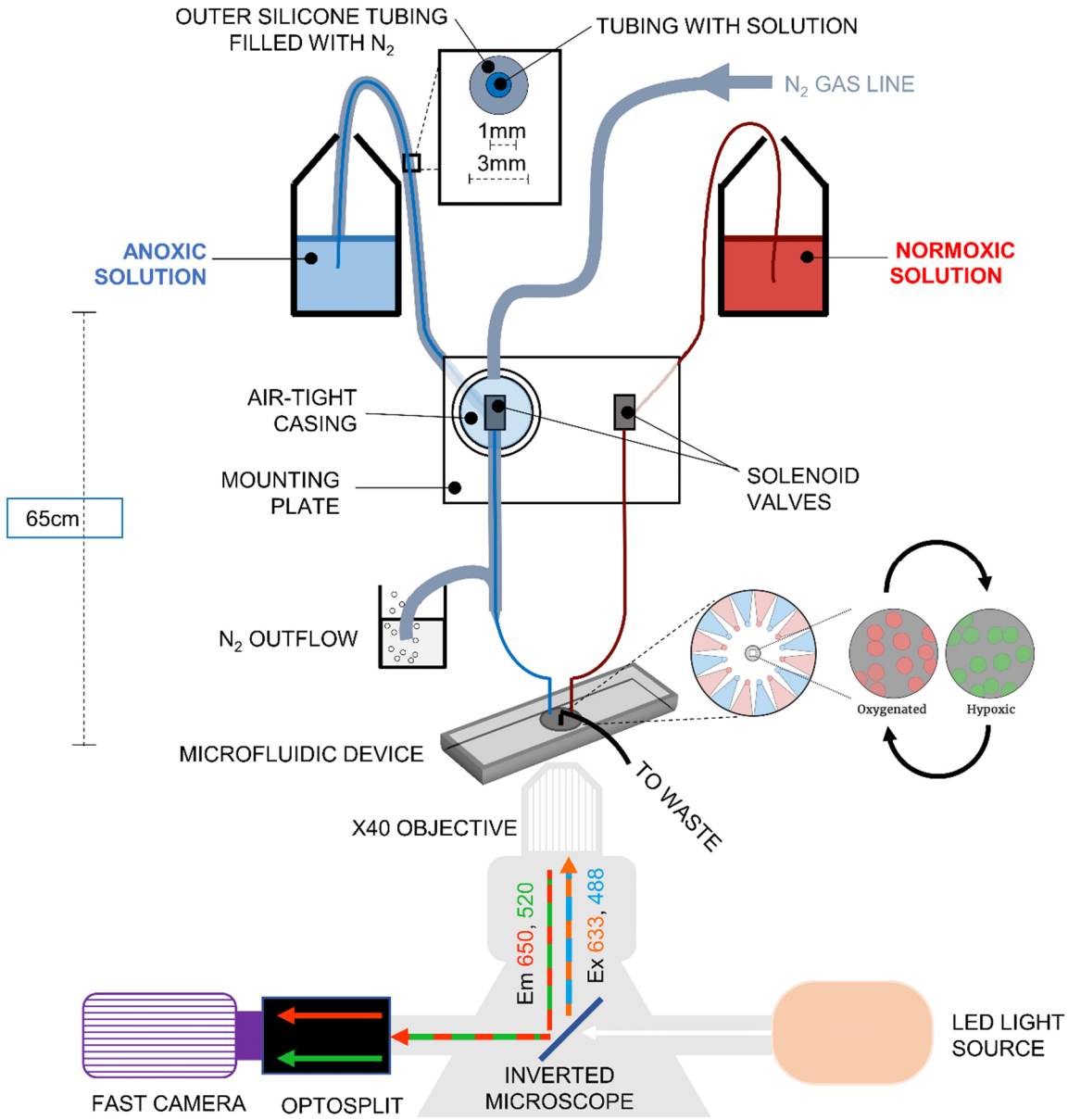

Supplementary Figure S1: Schematic figure of the setup for single-cell oxygen saturation imaging. Hepes-buffered Tyrode solutions are gravity-fed down two lines from reservoirs, one of which is bubbled with N_2 gas and contained 2 mM dithionite to maintain an anoxic environment. The anoxic line is protected from atmospheric O_2 ingress by an outer tube filled with N_2. Flow in the lines is controlled by computer-operated solenoid valves programmed to switch alternately. The solutions flow into a microfluidic chamber that passes microstreams to a central inspection window with a glass coverslip at the bottom. Cells are imaged through a x40 oil immersion objective, fixed to an inverted microscope (Leica DMi8). Excitation was provided by a LED light source (TL LED), that passed through a 640/488 dual bandpass filter (TRF59906-EM-LE ET-488/640). Fluorescence was collected and separated, using a Hamamatsu W-view Gemini beam splitter (Cairn; long pass T565lpxr-UF2 dichroic mirror), onto two fields of the camera view of a Hamamatsu W-view Gemini (Orca Flash 4.0LT) at 525 nm (bandpass ET525/50m) and >655 nm (ET655lp). Images were collected by HCI software and analysed by in-house MATLAB macros.

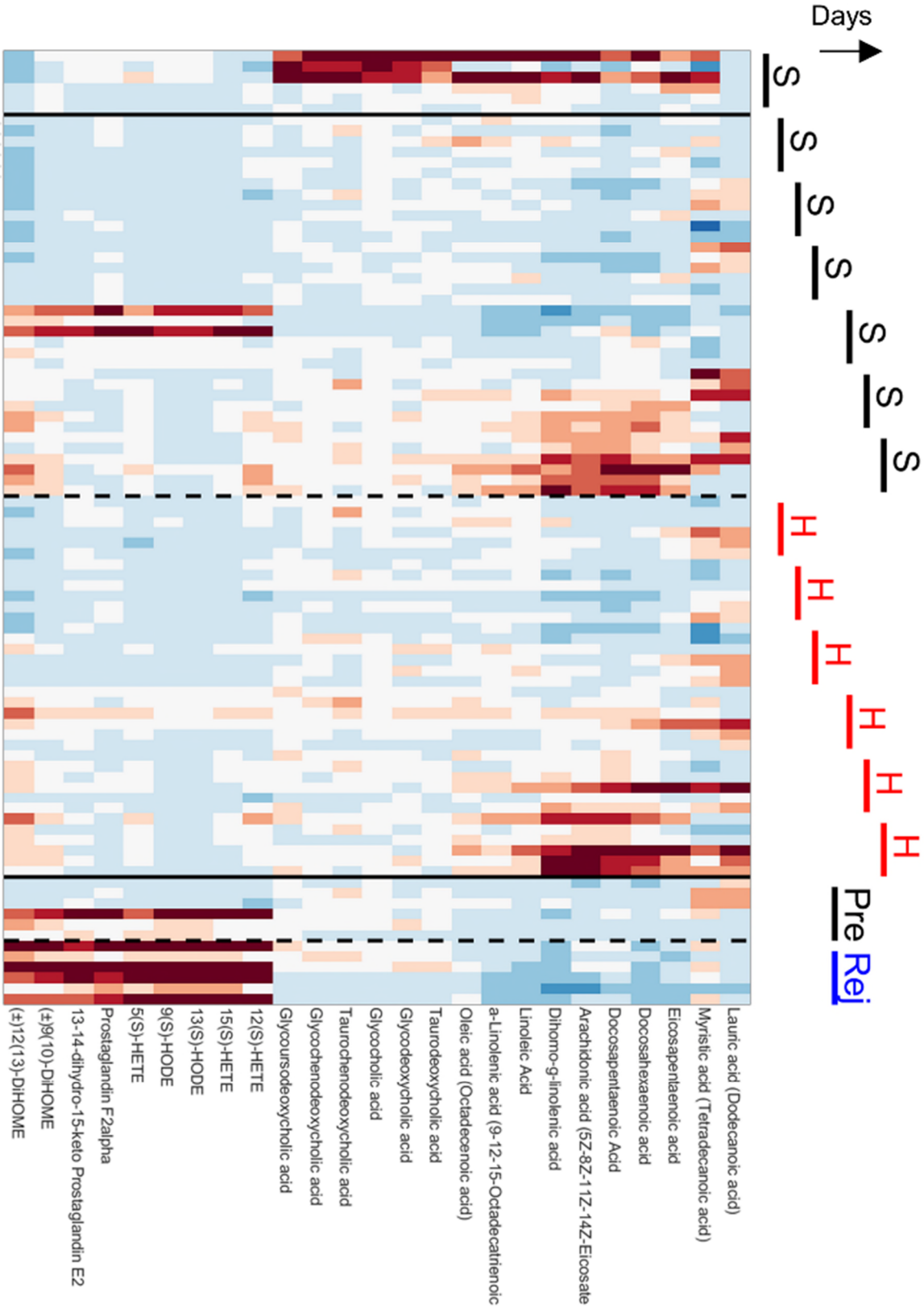

Supplementary Figure S2: Oxylipins. Heatmap shows oxylipins significantly affected by hypoxic storage or rejuvenation (two-way ANOVA: time and treatment with $P<0.05$).